Discrete Time-Crystalline Order Enabled by Quantum Many-Body Scars: Entanglement Steering via Periodic Driving

N. Maskara,[1] A. A. Michailidis,[2] W. W. Ho,[1,3] D. Bluvstein,[1] S. Choi,[4,5] M. D. Lukin,[1] and M. Serbyn[2]
[1]Department of Physics, Harvard University, Cambridge, Massachusetts 02138, USA
[2]IST Austria, Am Campus 1, 3400 Klosterneuburg, Austria
[3]Department of Physics, Stanford University, Stanford, California 94305, USA
[4]Department of Physics, University of California Berkeley, Berkeley, California 94720, USA
[5]Center for Theoretical Physics, Massachusetts Institute of Technology, Cambridge, Massachusetts 02139, USA

(Received 19 March 2021; accepted 26 May 2021; published 27 August 2021)

The control of many-body quantum dynamics in complex systems is a key challenge in the quest to reliably produce and manipulate large-scale quantum entangled states. Recently, quench experiments in Rydberg atom arrays [Bluvstein *et al.* Science **371**, 1355 (2021)] demonstrated that coherent revivals associated with quantum many-body scars can be stabilized by periodic driving, generating stable subharmonic responses over a wide parameter regime. We analyze a simple, related model where these phenomena originate from spatiotemporal ordering in an effective Floquet unitary, corresponding to discrete time-crystalline behavior in a prethermal regime. Unlike conventional discrete time crystals, the subharmonic response exists only for Néel-like initial states, associated with quantum scars. We predict robustness to perturbations and identify emergent timescales that could be observed in future experiments. Our results suggest a route to controlling entanglement in interacting quantum systems by combining periodic driving with many-body scars.

DOI: 10.1103/PhysRevLett.127.090602

Introduction.—Creating and manipulating entanglement is a fundamental goal of quantum information science, with broad implications in computation, metrology, and beyond. At the same time, not all forms of entanglement are useful. Strongly interacting quantum many-body systems generate large amounts of entanglement under their intrinsic dynamics, in a process known as thermalization [1,2]. However, such dynamics irreversibly scramble quantum information. Controlling entanglement while combating thermalization [3–5] in isolated interacting many-body systems [6–8] is therefore essential for applications of large-scale entangled states [9,10].

Experimental studies involving programmable quantum simulators based on Rydberg atom arrays [11] have suggested that interacting quantum systems can exhibit a weak breakdown of thermalization, where certain initial conditions exhibit surprising, persistent many-body revivals. This phenomenon comes from quantum many body scars (QMBS) [12,13]—anomalous, nonthermal eigenstates—named in analogy to nonergodic states in the spectrum of otherwise chaotic single particle Hamiltonians [14]. Intriguingly, in some models with QMBS the system undergoes periodic entanglement and disentanglement cycles [13,15–17], providing a potential route to the controlled manipulation of entanglement dynamics. In practice, however, QMBS are fragile [12,15,18,19]; since they rely on a dynamically disconnected subspace of nonthermalizing eigenstates [5,15,20–22], additional interactions generically lead to thermalization [19].

Recent experiments [23] demonstrated that periodic driving can dramatically increase the lifetime of scarred oscillations. This observation is surprising, since the driving frequencies used were resonant with the local energy scale, permitting easy energy absorption and rapid heating towards a featureless, infinite-temperature state. Additionally, the experiment observed a robust subharmonic response at half of the driving frequency, suggestive of discrete time-crystalline (DTC) order [24,25].

In this Letter, we propose a theoretical framework for understanding these experimental observations by introducing a mechanism whereby driving stabilizes quantum scarred oscillations, prolonging their lifetime and protecting them against arbitrary perturbations. Specifically, we focus on the PXP model [11,26,27] with kicked driving, an idealized model for the Rydberg atom array experiment [23]. This model exhibits robust subharmonic responses and many-body revivals coming from an effective many-body spin echo. The deviation from a perfect echo introduces a small parameter, allowing us to derive an effective prethermal description of the Floquet dynamics which is stable up until parametrically long times [28].

Namely, we construct an effective Hamiltonian in a rotating frame, hosting an emergent $\mathbb{Z}_2$ symmetry, which is spontaneously broken in its gapped ground state manifold. In the laboratory frame, the system oscillates between the

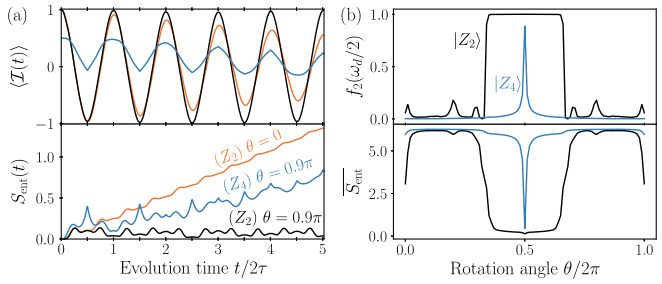

FIG. 1. (a) The density imbalance $\mathcal{I}$ and bipartite entanglement entropy characterize oscillations between the two Néel ordered states ($|Z_2\rangle$), for undriven (orange) and driven (black) dynamics in an infinite size chain simulated via iTEBD [37]. Adding driving with $\tau = 0.993\tau_r/2$ and $\theta = 0.9\pi$ to PXP model arrests the growth of entanglement entropy $S_{\rm ent}$ and prolongs the lifetime. In contrast, driven dynamics from the $|Z_4\rangle = |\bullet\circ\circ\circ\bullet\circ\circ\circ\ldots\rangle$ state, which do not support scar oscillations, thermalize rapidly (blue). (b) Subharmonic weight and average entanglement entropy, computed over 400 cycles ($T = 400\tau$), for an $L = 28$ chain, and $\tau = 0.993\tau_r/2$. Dynamics from the $|Z_2\rangle$ state form a stable plateau around $\theta = \pi$. However from $|Z_4\rangle$, the response disappears for $\theta \neq \pi$.

two spontaneously broken ground states, resulting in a robust subharmonic response characteristic of DTC [28–30]. However, this subharmonic response is restricted only to Néel-like initial states which have a strong overlap with the ground state of the effective Hamiltonian—a property inherited from QMBS. Our model differs crucially from earlier works on homogenous time crystals in one dimension [31–34] and mean-field constructions [35], in that the trajectory being stabilized is generated by an interacting Hamiltonian, which produces nontrivial entanglement. Therefore, our construction opens a prospective route towards coherent control of entanglement dynamics.

Model and phenomenology.—We study a periodically kicked model $H(t) = H_{\rm PXP} + \theta N \sum_{k\in\mathbb{Z}} \delta(t - k\tau)$, which generates the following one-period Floquet unitary,

$$U_F(\theta, \tau) = e^{-i\theta N} e^{-i\tau H_{\rm PXP}}, \tag{1}$$

$$H_{\rm PXP} = \sum_{i=1}^{L} P_{i-1}\sigma_i^x P_{i+1}, \qquad N = \sum_{i=1}^{L} n_i, \tag{2}$$

describing evolution with the PXP Hamiltonian $H_{\rm PXP}$ [11,26,27] for time τ, followed by the number operator N applied through rotation angle θ. For simplicity, the model is defined on a 1D chain of L sites with periodic boundaries, although much of the analysis carries over to higher dimensional bipartite lattices. Each site is a two-level system spanned by a ground ($\circ$) and an excited ($\bullet$) state. Operators $n_i = |\bullet\rangle\langle\bullet|_i$ and $P_i = |\circ\rangle\langle\circ|_i$ are projectors, while $\sigma_i^x = |\circ\rangle\langle\bullet|_i + |\bullet\rangle\langle\circ|_i$ generates Rabi oscillations. In the Hamiltonian, σ_i^x is dressed by projectors on neighboring sites, ensuring that dynamics remain within the blockaded subspace where adjacent sites are never simultaneously excited.

For $\theta = 0$ the Floquet dynamics (1) are equivalent to undriven evolution under $H_{\rm PXP}$. The PXP model is nonintegrable and features rapid growth of bipartite entanglement entropy, $S_{\rm ent}(t) = -{\rm tr}\rho\ln\rho$, where ρ is the half-chain density matrix, from the majority of product states. In contrast, quenching from the Néel state $|Z_2\rangle = |\bullet\circ\bullet\circ\ldots\rangle$ leads to coherent oscillations between $|Z_2\rangle$ and its inversion partner $|Z_2'\rangle$, as first seen in Ref. [11], with oscillation period $\tau_r \approx 1.51\pi$ that sets an intrinsic resonant timescale. These oscillations, supported on quantum scars [12], are captured by the sublattice imbalance in excitation number, $\mathcal{I} = (2/L)\sum_{i=1}^{L/2}(n_{2i-1} - n_{2i})$, see Fig. 1(a), and also occur in higher dimensional bipartite lattices [23,36]. However, dynamics under $H_{\rm PXP}$ generate entanglement, and the coherent many-body oscillations eventually decay.

The addition of strong driving with $\theta \approx \pi$ suppresses thermalization at early times, most clearly seen in the nominal growth of entanglement entropy over multiple cycles; see Fig. 1(a). Concomitantly, oscillations of $\mathcal{I}$ synchronize to half the drive frequency, a phenomenon known as subharmonic locking. The origin of this response is related to the existence of a special point at $\theta = \pi$, where driving implements an effective many-body echo; because $H_{\rm PXP}$ anticommutes with the operator $\mathcal{C} = \prod_i \sigma_i^z = e^{-i\pi N}$, then $U_F(\pi, \tau)^2 = \mathcal{C}e^{-i\tau H_{\rm PXP}}\mathcal{C}e^{-i\tau H_{\rm PXP}} = e^{i\tau H_{\rm PXP}}e^{-i\tau H_{\rm PXP}} = \mathbb{1}$, implying perfect subharmonic revivals across the *entire* Hilbert space. Furthermore, note that $H_{\rm PXP}$ anticommutes with $\mathcal{C}$, irrespective of the lattice geometry. However, upon deviating from $\theta = \pi$, these revivals rapidly damp out for typical initial states, whose undriven dynamics do not exhibit many-body oscillations in $\mathcal{I}$; see Fig. 1 and the Supplemental Material [37].

In contrast, long-lived oscillations from the Néel state persist over a wide range of parameters centered at $\theta = \pi$ and $\tau = \tau_r/2$. To quantify the response, we compute the subharmonic weight $f_2(\omega_d/2) \propto |S(\omega_d/2)|^2$, defined as the normalized spectral weight of $\langle \mathcal{I}(t) \rangle$ at half the driving frequency $\omega_d = 2\pi/\tau$, rescaled so $f_2(\omega_d/2) = 1$ for perfect subharmonic response at $\theta = \pi$ from the Néel states; see Supplemental Material [37]. The plateaus in the subharmonic weight and time-averaged entanglement entropy in Fig. 1(b) signal a robust, persistent response at $\omega_d/2$.

Many-body echo in su(2) subspace.—The robust subharmonic response can be qualitatively understood using mean-field-like trajectories on an effective Bloch sphere. We invoke the forward-scattering approximation (FSA), which constructs an $L + 1$ dimensional subspace that captures dynamics under $H_{\rm PXP}$ from a Néel initial state, and approximate su(2) algebraic structure [12] of a spin-$L/2$ collective degree of freedom. The S^z operator is defined by the density imbalance, $S^z = \sum_{i=1}^{L/2}(n_{2i-1} - n_{2i})$, so the Néel state $|Z_2\rangle$ ($|Z_2'\rangle$) corresponds to the North (South) pole. The S^x operator is approximately proportional to $H_{\rm PXP}$, and

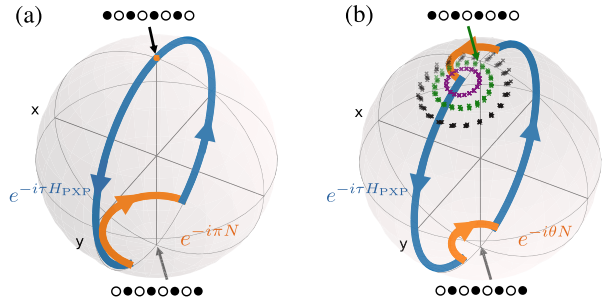

FIG. 2. Trajectories of driven PXP model for $L = 16$, plotted on the Bloch sphere of the collective spin $L/2$. (a) The dynamics generated by two periods of $U_F(\pi, \tau)$ exhibit a perfect return to the $|Z_2\rangle$ initial state: $e^{-i\tau H_{\mathrm{PXP}}}$ with $\tau = 0.45\tau_r$ underrotates the $|Z_2\rangle$ state (blue line), then the application of $e^{-i\pi N}$ (orange line) flips the x, y projections of the spin so that the second Floquet pulse completes the cycle. (b) The same dynamics but for $\theta = \pi - 0.05$ supports a periodic trajectory near the Néel state. Dynamics initialized near the periodic trajectory precess around it at stroboscopic times forming cycles depicted for 100 driving periods for three initial states (green ring corresponds to $|Z_2\rangle$ initialization).

generates a rotation that exchanges the two Néel states (blue lines in Fig. 2). Finally, S^y is calculated using su(2) commutation relations. In contrast, the action of $e^{-i\theta N}$ pulses is more complex, since the operator N does not have a closed form representation in the su(2) subspace. However, it can be approximated as $N \sim (S^z)^2$ in the vicinity of the Néel states $|Z_2\rangle$ and $|Z_2'\rangle$, which accumulate identical phases under $e^{-i\theta N}$, see Ref. [37] and Fig. 2(b). Note that we use the weakly deformed PXP model [15] to generate spin operators, but consider dynamics under H_{PXP} [37].

We visualize the many-body dynamics by computing expectation values of the collective spin operators $S^{x,y,z}$. Figure 2(a) illustrates that at $\theta = \pi$ the second application of H_{PXP} returns the system to its initial state. Away from $\theta = \pi$, trajectories from $|Z_2\rangle$ are no longer closed, but there exists a nearby closed orbit with period 2τ, see Fig. 2(b). States near this periodic orbit, including the Néel state, exhibit stroboscopic precession around the fixed point, explaining subharmonic response. In this picture, the existence of periodic trajectories is qualitatively similar to mean-field descriptions of time crystals [35,45,46]. However, a key difference is that the emergent spin-$L/2$ degree of freedom is not composed of independent spins, evinced by nontrivial entanglement oscillations. Furthermore, dynamics outside of collective spin-$L/2$ subspace are ergodic, leading to rapid thermalization from other initial states. As such, this picture does not explain why the spin-$L/2$ subspace is a good approximation, and how driving reduces thermalization, for which we must consider the many-body Floquet unitary.

Prethermal analysis and effective Hamiltonian.—We analyze the many-body dynamics by expanding around the perfect echo point $\theta = \pi$ where the Floquet unitary is denoted $\mathcal{X}_\tau = U_F(\pi, \tau)$. This allows us to write

$$U_F(\theta, \tau) = e^{i\epsilon N}\mathcal{X}_\tau, \quad \epsilon = \pi - \theta, \tag{3}$$

where ϵ is a small parameter quantifying the deviation from the perfect point. Since $\mathcal{X}_\tau^2 = \mathbb{1}$, the dynamics are equivalent to a generalized spin flip, followed by short evolution under N for time ϵ [37]. As such, the unitary $U_F(\theta, \tau)$ is written in the canonical time crystal form [25,29]; here, we apply the techniques from Refs. [28,38] to show the Floquet unitary can be approximated by $U_F \approx \mathcal{V}e^{-i\epsilon H_F}\mathcal{X}_\tau\mathcal{V}^\dagger$, where H_F is an effective Hamiltonian constructed perturbatively in ϵ, and $\mathcal{V}$ is a perturbative frame transformation [37].

As the DTC phenomenology depends on spectral properties of the effective Floquet unitary, we base our analysis on the leading order effective Hamiltonian and Floquet unitary,

$$H_F^{(1)} = -\frac{1}{2}(N + \mathcal{X}_\tau N \mathcal{X}_\tau), \quad U_F^{(1)}(\theta, \tau) \equiv e^{-i\epsilon H_F^{(1)}}\mathcal{X}_\tau. \tag{4}$$

The effective Hamiltonian $H_F^{(1)}$ corresponds to the average Hamiltonian in a frame corotating with $\mathcal{X}_\tau$, and so to leading order ϵ sets the timescale of dynamics in the rotating frame. Crucially, the expansion of H_F has an emergent $\mathbb{Z}_2$ symmetry $[H_F, \mathcal{X}_\tau] = 0$ at higher orders as well, which ultimately comes from time periodicity of the drive [28,37]; nevertheless, formally the expansion is an asymptotic series, and hence should be truncated at some optimal order to accurately capture dynamics of local observables. The effect of residual terms is rigorously bounded [28,39], guaranteeing accuracy of H_F up to the prethermal timescale $T_p \gtrsim (\tau/\epsilon)e^{c_p/\epsilon}$ for some $c_p > 0$.

The origin of the subharmonic response can be understood by analyzing eigenstates of the transformed Floquet unitary in Eq. (4) and their dimensionless quasienergies ε, defined by $U_F^{(1)}|u\rangle = e^{i\varepsilon}|u\rangle$. For τ near an integer multiple of $\tau_r/2$, the Floquet operator has a pair of eigenstates characterized by strong overlap with $|Z_2\rangle, |Z_2'\rangle$, and featuring nearly degenerate quasienergies (0 pairing) or quasienergies separated by π (π pairing), see Fig. 3(a). These observations imply the eigenstates can be well approximated by the long-range correlated "cat" states $|\pm\rangle = (|Z_2\rangle \pm |Z_2'\rangle)/\sqrt{2}$ as these states carry definite momentum k_0 ($|+\rangle$) and k_π ($|-\rangle$), and underlie spontaneous symmetry breaking (SSB) of the system's translation symmetry. However, the emergent symmetries $\mathcal{X}_\tau$ also play a crucial role, as the π and 0 quasienergy gaps occur when $\mathcal{X}_\tau$ either exchanges the two Néel states ($\tau = \tau_r/2$) or leaves them invariant ($\tau = 0, \tau_r$). A π quasienergy gap between the cat states $|\pm\rangle$ leads to subharmonic response in dynamics from the $|Z_2\rangle$ or $|Z_2'\rangle$ state, and is characteristic of time-crystalline order [25,29,47–49]. At the level of the effective

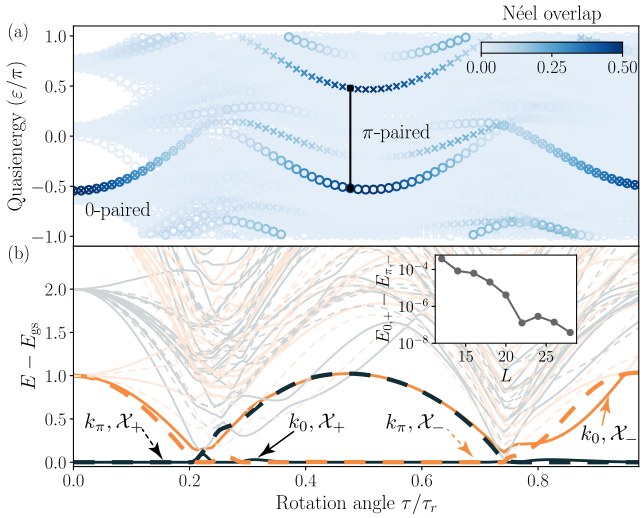

FIG. 3. (a) Eigenspectrum of $U_F^{(1)}$ plotted for various rotation angles τ, $L = 16$, and $\epsilon = 1$, with color intensity reflecting overlap with the Néel state. Near $\tau/\tau_r \approx 1/2$, the states with the largest overlap exhibit π pairing, indicating subharmonic response. However, near $\tau/\tau_r \approx 0, 1$, they exhibit 0 pairing. (b) Low-energy spectrum of $H_F^{(1)}$ reveals twofold degeneracy between ground states from $k = 0$ and π momentum sectors (denoted as $k_{0,\pi}$) with $\mathcal{X}_\tau$ eigenvalues $\pm 1 (\mathcal{X}_\pm)$ in the region that corresponds to π pairing in (a). The splitting of the ground state manifold vanishes exponentially with system size within the paired regions, with the inset showing finite size scaling at $\tau/\tau_r = 1/2$.

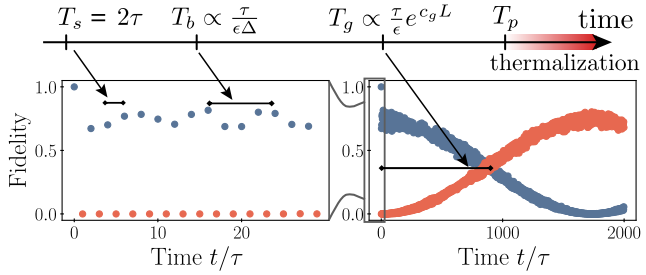

FIG. 4. Dynamics of revival fidelity under the periodically kicked Rydberg Hamiltonian, and emergent prethermal timescales. Stroboscopic dynamics of fidelity for $\theta = 1.1\pi$, and $\tau = 0.993\tau_r/2$ reveal the subharmonic timescale T_s, the beating timescale T_b, and Rabi oscillations in the ground space, with characteristic timescale T_g. Even (odd) multiples of τ are colored blue (red). Data are for the $L = 14$ chain.

Hamiltonian $H_F^{(1)}$, these $\pi(0)$-paired eigenstates correspond to degenerate ground states in Fig. 3(b), separated by a finite gap Δ to excited states, and belonging to different (same) symmetry sectors of $\mathcal{X}_\tau$. Hence $\mathcal{X}_\tau$ symmetry breaking in the ground state is linked to DTC order and the subharmonic oscillations of spatial order [25,29,37].

We argue the observed region with DTC order descends from a model with conjectured perfect scars [15,37]. Specifically, if we deform the PXP model as described in Ref. [15], $\mathcal{X}_\tau$ at $\tau = \tau_r/2$ exactly exchanges the Néel states, and $|\pm\rangle$ become true ground states of $H_F^{(1)}$ with a constant gap $\Delta \geq 1$. The PXP model, as well as driving for τ away from $\tau_r/2$, are weak deformations of this drive. However, these deformations do not preserve the emergent symmetry $\mathcal{X}_\tau$ at the level of $H_F^{(1)}$, and could destroy the ground state degeneracy. In the Supplemental Material [37], we argue that since the emergent symmetry changes slowly as we deform the drive, the ground states throughout the π-paired region in Fig. 3 may be adiabatically connected to $|\pm\rangle$. Indeed, we confirm the energy splitting in the ground state of $H_F^{(1)}$ decreases exponentially with system size, see Fig. 3(b) inset, as expected for SSB.

The above analysis reveals four distinct timescales emergent in the prethermal regime of Eq. (4). The shortest timescale $T_s = 2\tau$ is the subharmonic response. The second timescale, determined by the gap Δ in the spectrum of $H_F^{(1)}$, is $T_b \propto \tau(\epsilon\Delta)^{-1}$ and comes from overlap between the Néel initial state and the lowest lying excited states. Semiclassically, T_b is the precession period from Fig. 2(b). Finally, the longest timescale is set by the inverse energy splitting in the ground state manifold of $H_F^{(1)}$, $T_g \propto (\tau/\epsilon)e^{c_d L}$, characteristic of SSB. All phenomenology is ultimately contingent upon the validity of the prethermal analysis, which holds until $T_p \gtrsim (\tau/\epsilon)e^{c_p/\epsilon}$.

Connections to experiments.—Going beyond the idealized model (1), we replace H_{PXP} in Eq. (2) by the Rydberg Hamiltonian $H_{\mathrm{Ry}} = (\Omega/2)\sum_i \sigma_i^x - \delta\sum_i n_i + \sum_i (V_1 n_i n_{i+1} + V_2 n_i n_{i+2})$, which includes imperfect Rydberg blockade and next-nearest-neighbor interactions. The PXP Hamiltonian is recovered from H_{Ry} in the limit $V_1 \to \infty, V_2 = 0$, and the resonant time $\tau_r \propto 1/\Omega$ is rescaled by Ω. Here, we consider a 1D chain with $V_2 = V_1/2^6, V_1 = 10\Omega$, and choose $\delta = V_2$ to cancel the static background from the next-nearest-neighbor interactions [23].

Figure 4 illustrates the timescales T_s, T_b, and T_g from stroboscopic dynamics of the revival fidelity $F_n = |\langle Z_2|U_F(\theta,\tau)^n|Z_2\rangle|^2$ generated by the kicked Hamiltonian $H(t) = H_{\mathrm{Ry}} + \theta N \sum_k \delta(t - k\tau)$. Over tens of driving cycles, we observe a robust subharmonic response, and an emergent beating timescale T_b. Over hundreds of driving cycles, we observe slow oscillations between even periods F_{2n} and odd periods F_{2n+1}, with timescale T_g. Specifically, in the rotating frame, the two ground states of H_F, $\approx|\pm\rangle$, form an effective two-level system with energy splitting $\Delta E = E_+ - E_-$. The initial state can be expanded as $|Z_2\rangle \equiv (|+\rangle + |-\rangle)/\sqrt{2}$, and after a time $T_g = \pi/(2\Delta E)$, it evolves into a superposition $(|+\rangle + i|-\rangle)/\sqrt{2}$ equivalent to $(|Z_2\rangle - i|Z_2'\rangle)/\sqrt{2}$ modulo global phase, which is a macroscopic superposition corresponding to the so-called Greenberger-Horne-Zeilinger (GHZ) state. Dynamics in

the lab frame are related by $\mathcal{X}_\tau$ kicks, which exchange the Néel states every period. Finally, the prethermal time, when all fidelities may become exponentially small in L, is not visible for the system sizes or times simulated.

Discussion.—These considerations demonstrate that entanglement dynamics associated with quantum many-body scars can be stabilized and steered in the periodically kicked PXP model, resulting in an evolution strongly reminiscent of prethermal DTC order. Our construction relies on the effective many-body π pulse realized through quantum scars, which connect the two Néel states via an entangled trajectory, and a driving pulse that reverses the direction of time. Similar to prethermal time crystals, the emergent order features a robust, long-lived subharmonic response and spatiotemporal order for a range of parameters. However, in our model these signatures are present only for eigenstates that are perturbatively close to the Néel initial state, and require sufficiently high fidelity state preparation to be observed [32]. Nevertheless, we demonstrate that the signatures of DTC physics survive in an experimentally relevant model, thus providing a possible explanation for recent experimental observations in Ref. [23]. Moreover, we theoretically predict new emergent timescales that could be observed in future experiments and the possibility of preparing GHZ states [40] in driven quench dynamics.

The phenomenon described here drastically enhances the stability of nonergodic dynamics thus opening a large number of exciting directions. Specifically, by extending this construction to the more complicated trajectories in the PXP model [16] or to quantum scars in other models [5,17,22,50,51], control over more complex entanglement dynamics could be implemented. From a practical perspective, there remain a number of questions related to experiments in Rydberg arrays [23]. In particular, it is desirable to understand the dynamics in two-dimensional lattices [36], including the situations where two sublattices have different numbers of nearest neighbors. In higher dimensions, there exists an intriguing possibility of realizing a true prethermal time crystal, with a finite temperature phase transition in H_F. It is also desirable to build a theory for higher order subharmonic responses observed in experiments [23], and obtain analytical understanding for continuously driven models. Finally, it is important to understand if one can implement full control over the many-body dynamics within the effective spin-$L/2$ subspace [52], which could be utilized for applications such as robust quantum information storage and quantum metrology.

We thank Dmitry Abanin, Ehud Altman, Iris Cong, Sepehr Ebadi, Alex Keesling, Harry Levine, Ahmed Omran, Hannes Pichler, Rhine Samajdar, Guilia Semeghini, Tout Wang, Norman Yao, and Harry Zhou for stimulating discussions. We acknowledge support from the Center for Ultracold Atoms, the National Science Foundation, the Vannevar Bush Faculty Fellowship, the U.S. Department of Energy, the Army Research Office MURI, and the DARPA ONISQ program (M. L., N. M, W. W. H., D. B.); the European Research Council (ERC) under the European Union's Horizon 2020 Research and Innovation Programme Grant Agreement No. 850899 (A. M. and M. S.); the Department of Energy Computational Science Graduate Fellowship under Awards No. DE-SC0021110 (N. M.); the Moore Foundation EPiQS initiative Grant No. GBMF4306, the National University of Singapore (NUS) Development Grant AY2019/2020 and the Stanford Institute for Theoretical Physics (W. W. H.); the NSF Graduate Research Fellowship Program (Grant No. DGE1745303) and The Fannie and John Hertz Foundation (D. B.); the Miller Institute for Basic Research in Science (S. C.); DOE Quantum Systems Accelerator – Contract No. 7568717; and DOE Programmable Quantum Simulators for Lattice Gauge Theories and Gauge-Gravity Correspondence – Grant No. DE-SC0021013.

[1] L. D'Alessio, Y. Kafri, A. Polkovnikov, and M. Rigol, From quantum chaos and eigenstate thermalization to statistical mechanics and thermodynamics, Adv. Phys. **65**, 239 (2016).

[2] A. M. Kaufman, M. E. Tai, A. Lukin, M. Rispoli, R. Schittko, P. M. Preiss, and M. Greiner, Quantum thermalization through entanglement in an isolated many-body system, Science **353**, 794 (2016).

[3] D. A. Abanin, E. Altman, I. Bloch, and M. Serbyn, Colloquium: Many-body localization, thermalization, and entanglement, Rev. Mod. Phys. **91**, 021001 (2019).

[4] R. Nandkishore and D. A Huse, Many-body localization and thermalization in quantum statistical mechanics, Annu. Rev. Condens. Matter Phys. **6**, 15 (2015).

[5] M. Serbyn, D. A. Abanin, and Z. Papić, Quantum many-body scars and weak breaking of ergodicity, arXiv:2011.09486.

[6] I. Bloch, J. Dalibard, and W. Zwerger, Many-body physics with ultracold gases, Rev. Mod. Phys. **80**, 885 (2008).

[7] I. M. Georgescu, S. Ashhab, and F. Nori, Quantum simulation, Rev. Mod. Phys. **86**, 153 (2014).

[8] A. Browaeys and T. Lahaye, Many-body physics with individually controlled Rydberg atoms, Nat. Phys. **16**, 132 (2020).

[9] R. Horodecki, P. Horodecki, M. Horodecki, and K. Horodecki, Quantum entanglement, Rev. Mod. Phys. **81**, 865 (2009).

[10] L. Pezzè, A. Smerzi, M. K. Oberthaler, R. Schmied, and P. Treutlein, Quantum metrology with nonclassical states of atomic ensembles, Rev. Mod. Phys. **90**, 035005 (2018).

[11] H. Bernien, S. Schwartz, A. Keesling, H. Levine, A. Omran, H. Pichler, S. Choi, A. S. Zibrov, M. Endres, M. Greiner, V. Vuletic, and M. D. Lukin, Probing many-body dynamics on a 51-atom quantum simulator, Nature (London) **551**, 579 (2017).

[12] C. J. Turner, A. A. Michailidis, D. A. Abanin, M. Serbyn, and Z. Papić, Weak ergodicity breaking from quantum many-body scars, Nat. Phys. **14**, 745 (2018).
[13] W. W. Ho, S. Choi, H. Pichler, and M. D. Lukin, Periodic Orbits, Entanglement, and Quantum Many-Body Scars in Constrained Models: Matrix Product State Approach, Phys. Rev. Lett. **122**, 040603 (2019).
[14] E. J. Heller, Bound-State Eigenfunctions of Classically Chaotic Hamiltonian Systems: Scars of Periodic Orbits, Phys. Rev. Lett. **53**, 1515 (1984).
[15] S. Choi, C. J. Turner, H. Pichler, W. W. Ho, A. A. Michailidis, Z. Papić, M. Serbyn, M. D. Lukin, and D. A. Abanin, Emergent su(2) Dynamics and Perfect Quantum Many-Body Scars, Phys. Rev. Lett. **122**, 220603 (2019).
[16] A. A. Michailidis, C. J. Turner, Z. Papić, D. A. Abanin, and M. Serbyn, Slow Quantum Thermalization and Many-Body Revivals from Mixed Phase Space, Phys. Rev. X **10**, 011055 (2020).
[17] S. Chattopadhyay, H. Pichler, M. D. Lukin, and W. W. Ho, Quantum many-body scars from virtual entangled pairs, Phys. Rev. B **101**, 174308 (2020).
[18] V. Khemani, C. R. Laumann, and A. Chandran, Signatures of integrability in the dynamics of Rydberg-blockaded chains, Phys. Rev. B **99**, 161101(R) (2019).
[19] C.-J. Lin, A. Chandran, and O. I. Motrunich, Slow thermalization of exact quantum many-body scar states under perturbations, Phys. Rev. Research **2**, 033044 (2020).
[20] N. Shiraishi and T. Mori, Systematic Construction of Counterexamples to the Eigenstate Thermalization Hypothesis, Phys. Rev. Lett. **119**, 030601 (2017).
[21] S. Moudgalya, S. Rachel, B. A. Bernevig, and N. Regnault, Exact excited states of nonintegrable models, Phys. Rev. B **98**, 235155 (2018).
[22] S. Moudgalya, B. A. Bernevig, and N. Regnault, Quantum many-body scars in a Landau level on a thin torus, Phys. Rev. B **102**, 195150 (2020).
[23] D. Bluvstein, A. Omran, H. Levine, A. Keesling, G. Semeghini, S. Ebadi, T. T. Wang, A. A. Michailidis, N. Maskara, W. W. Ho, S. Choi, M. Serbyn, M. Greiner, V. Vuletić, and M. D. Lukin, Controlling quantum many-body dynamics in driven Rydberg atom arrays, Science **371**, 1355 (2021).
[24] V. Khemani, A. Lazarides, R. Moessner, and S. L. Sondhi, Phase Structure of Driven Quantum Systems, Phys. Rev. Lett. **116**, 250401 (2016).
[25] D. V. Else, B. Bauer, and C. Nayak, Floquet Time Crystals, Phys. Rev. Lett. **117**, 090402 (2016).
[26] P. Fendley, K. Sengupta, and S. Sachdev, Competing density-wave orders in a one-dimensional hard-boson model, Phys. Rev. B **69**, 075106 (2004).
[27] I. Lesanovsky and H. Katsura, Interacting Fibonacci anyons in a Rydberg gas, Phys. Rev. A **86**, 041601(R) (2012).
[28] D. V. Else, B. Bauer, and C. Nayak, Prethermal Phases of Matter Protected by Time-Translation Symmetry, Phys. Rev. X **7**, 011026 (2017).
[29] C. W. von Keyserlingk, V. Khemani, and S. L. Sondhi, Absolute stability and spatiotemporal long-range order in floquet systems, Phys. Rev. B **94**, 085112 (2016).
[30] N. Y. Yao, A. C. Potter, I.-D. Potirniche, and A. Vishwanath, Discrete Time Crystals: Rigidity, Criticality, and Realizations, Phys. Rev. Lett. **118**, 030401 (2017).
[31] B. Huang, Y.-H. Wu, and W. V. Liu, Clean Floquet Time Crystals: Models and Realizations in Cold Atoms, Phys. Rev. Lett. **120**, 110603 (2018).
[32] A. Pizzi, D. Malz, G. D. Tomasi, J. Knolle, and A. Nunnenkamp, Time crystallinity and finite-size effects in clean Floquet systems, Phys. Rev. B **102**, 214207 (2020).
[33] B. Mukherjee, S. Nandy, A. Sen, D. Sen, and K. Sengupta, Collapse and revival of quantum many-body scars via Floquet engineering, Phys. Rev. B **101**, 245107 (2020).
[34] H. Yarloo, A. E. Kopaei, and A. Langari, Homogeneous Floquet time crystal from weak ergodicity breaking, Phys. Rev. B **102**, 224309 (2020).
[35] A. Russomanno, F. Iemini, M. Dalmonte, and R. Fazio, Floquet time crystal in the Lipkin-Meshkov-Glick model, Phys. Rev. B **95**, 214307 (2017).
[36] A. A. Michailidis, C. J. Turner, Z. Papić, D. A. Abanin, and M. Serbyn, Stabilizing two-dimensional quantum scars by deformation and synchronization, Phys. Rev. Research **2**, 022065(R) (2020).
[37] See Supplemental Material at http://link.aps.org/supplemental/10.1103/PhysRevLett.127.090602 for more information on the subharmonic weight, FSA construction, derivation of prethermal Hamiltonian and gap in its spectrum, and for simulations with more realistic Rydberg Hamiltonian, which also includes Refs. [12,15,23, 35,36,38–44].
[38] D. V. Else, W. W. Ho, and P. T. Dumitrescu, Long-Lived Interacting Phases of Matter Protected by Multiple Time-Translation Symmetries in Quasiperiodically Driven Systems, Phys. Rev. X **10**, 021032 (2020).
[39] D. Abanin, W. D. Roeck, W. W. Ho, and F. Huveneers, A rigorous theory of many-body prethermalization for periodically driven and closed quantum systems, Commun. Math. Phys. **354**, 809 (2017).
[40] A. Omran *et al.*, Generation and manipulation of Schrödinger cat states in Rydberg atom arrays, Science **365**, 570 (2019).
[41] J. R. Johansson, P. D. Nation, and F. Nori, Qutip 2: A python framework for the dynamics of open quantum systems, Comput. Phys. Commun. **184**, 1234 (2013).
[42] C. J. Turner, A. A. Michailidis, D. A. Abanin, M. Serbyn, and Z. Papić, Quantum scarred eigenstates in a Rydberg atom chain: Entanglement, breakdown of thermalization, and stability to perturbations, Phys. Rev. B **98**, 155134 (2018).
[43] M. B. Hastings, Locality in quantum systems, arXiv:1008.5137.
[44] M. B. Hastings and X.-G. Wen, Quasiadiabatic continuation of quantum states: The stability of topological ground-state degeneracy and emergent gauge invariance, Phys. Rev. B **72**, 045141 (2005).
[45] S. Choi, J. Choi, R. Landig, G. Kucsko, H. Zhou, J. Isoya, F. Jelezko, S. Onoda, H. Sumiya, V. Khemani, C. von Keyserlingk, N. Y. Yao, E. Demler, and M. D. Lukin, Observation of discrete time-crystalline order in a disordered dipolar many-body system, Nature (London) **543**, 221 (2017).

[46] W. W. Ho, S. Choi, M. D. Lukin, and D. A. Abanin, Critical Time Crystals in Dipolar Systems, Phys. Rev. Lett. **119**, 010602 (2017).

[47] V. K. Kozin and O. Kyriienko, Quantum Time Crystals from Hamiltonians with Long-Range Interactions, Phys. Rev. Lett. **123**, 210602 (2019).

[48] V. Khemani, R. Moessner, and S. L. Sondhi, Comment on quantum time crystals from Hamiltonians with long-range interactions, arXiv:2001.11037.

[49] A. Pizzi, J. Knolle, and A. Nunnenkamp, Higher-order and fractional discrete time crystals in clean long-range interacting systems, Nat. Commun. **12**, 2341 (2021).

[50] K. Bull, I. Martin, and Z. Papić, Systematic Construction of Scarred Many-Body Dynamics in 1d Lattice Models, Phys. Rev. Lett. **123**, 030601 (2019).

[51] K. Mizuta, K. Takasan, and N. Kawakami, Exact Floquet quantum many-body scars under Rydberg blockade, Phys. Rev. Research **2**, 033284 (2020).

[52] A. Lerose, J. Marino, A. Gambassi, and A. Silva, Prethermal quantum many-body Kapitza phases of periodically driven spin systems, Phys. Rev. B **100**, 104306 (2019).